Advanced Radiomics for Predicting Extracapsular Invasion of Metastatic Axillary Lymph Nodes in Breast Cancer Patients Using CT Imaging

Erkan Bilgin, Ezel Yaltirik Bilgin, Ahmet Bayrak and Sahap Torenek

Department of Radiology, Dr. Abdurrahman Yurtaslan Ankara Oncology Training and Research Hospital, Yenimahalle, Ankara, Turkiye

ABSTRACT

Objective: To evaluate the efficacy of radiomics features extracted from computed tomography (CT) images in predicting extracapsular invasion (ECI) of metastatic axillary lymph nodes in breast cancer patients.

Study Design: Observational study.

Place and Duration of the Study: Department of Radiology, Dr. Abdurrahman Yurtaslan Ankara Oncology Training and Research Hospital, Yenimahalle, Ankara, Turkiye, from January 2019 to 2024.

Methodology: Female patients diagnosed with breast cancer and axillary lymph node involvement were retrospectively reviewed. High-dimensional radiomics features were extracted from CT images, including morphology, histogram, gray level co-occurrence matrix (GLCM), gray level run length matrix (GLRLM), neighbouring gray tone difference matrix (NGTDM), and gray level size zone matrix (GLSZM) features. Advanced statistical methods, including the Mann-Whitney U test, LASSO, and ANOVA, were employed to identify significant predictors of ECI. Logistic regression models were developed, and their performance was evaluated using ROC curve analysis.

Results: The study identified 39 radiomics features significantly associated with ECI ($p < 0.05$). Integrating multiple radiomics features, the combined model demonstrated adequate diagnostic performance. The model explained 57.8% of the variance in ECI status according to the Nagelkerke R-square statistic. Individual feature models' predictive power was lower than the combined model.

Conclusion: Radiomics features derived from CT images provide a powerful non-invasive tool for predicting ECI in metastatic axillary lymph nodes due to breast cancer. The combined model's superior performance underscores the importance of a multifaceted approach in medical imaging analysis. These findings highlight the potential for radiomics to enhance prognostic assessments and guide personalised treatment strategies in breast cancer management.

Key Words: *Radiomics, Breast cancer, Axillary lymph node involvement, Extracapsular invasion, Computed tomography, Predictive modelling.*

How to cite this article: Bilgin E, Bilgin EY, Bayrak A, Torenek S. Advanced Radiomics for Predicting Extracapsular Invasion of Metastatic Axillary Lymph Nodes in Breast Cancer Patients Using CT Imaging. *J Coll Physicians Surg Pak* 2025; **35(04)**:415-419.

INTRODUCTION

Breast cancer remains a significant concern for women's health, with profound implications for morbidity and mortality. One of the critical factors in the staging and prognosis of breast cancer is the involvement of axillary lymph nodes.[1-4] Distant metastases and recurrences are more common in patients with axillary lymph involvement, that influences treatment decisions and patient outcomes. Among the various pathological features, extracapsular invasion (ECI) of the metastatic axillary lymph node is a critical point for aggressive diseases and a poorer prognosis.[5-8]

Correspondence to: Dr. Ezel Yaltirik Bilgin, Department of Radiology, Dr. Abdurrahman Yurtaslan Ankara Oncology Training and Research Hospital, Yenimahalle, Ankara, Turkiye
E-mail: ezelyaltirik@yahoo.com

Received: August 24, 2024; Revised: March 01, 2025; Accepted: April 03, 2025
DOI: https://doi.org/10.29271/jcpsp.2025.04.415

Advanced imaging techniques and computational analysis have opened new avenues for enhancing diagnostic accuracy and prediction of prognosis in cancer patients.[9,10] Radiomics, a burgeoning field within medical imaging, involves achieving and analysing quantitative information from medical images. These attributes, which contain various aspects of tumour shape, intensity, and texture, can supply valuable insights into the tumour microenvironment and behaviour that need to be discernible through conventional imaging interpretations.[11-16]

CT imaging is a widely used imaging technique in clinical practice for the evaluation of cancer patients, offering high-resolution images that facilitate detailed analysis of anatomical structures. This study focused on predicting the ECI of metastatic axillary lymph nodes due to breast cancer using radiomics features. By using radiomics, this study aimed to identify specific imaging biomarkers that correlate with ECI, thereby improving predictive accuracy and aiding in personalised treatment planning.

METHODOLOGY

This was an observational retrospective study and included 56 female patients with metastatic axillary lymph nodes positive

for breast cancer. All patients underwent computed tomography (CT) imaging as a part of their clinical evaluation from January 2019 to 2024. The inclusion standards were: Confirmed diagnosis of breast cancer with axillary lymph node involvement, availability of high-quality CT images, and histopathological confirmation of ECI status. The exclusion criteria were substandard quality or incomplete CT images, previous treatment history (surgery, chemotherapy, or radiotherapy) before the CT scan, and incomplete clinical or pathological data.

All patients underwent enhanced chest CT scan using a 16-slice multidetector CT scanner (GE Revolution, General Electric, Milwaukee, Wisconsin, USA). An experienced radiologist with a 15-year experience, manually delineated regions of interest (ROIs) encompassing the metastatic lymph nodes and a 3mm diameter around using LIFEx software. The segmentation of the lymph node and perinodal area are presented in Figure 1. A total of 89 radiomics features drew out from the ROIs.

SPSS (Statistical Package for the Social Sciences) version 26 (IBM Corp., Armonk, NY, USA) and R software (version 4.3.1) were used for statistical analysis. The distribution of continuous variables was evaluated using statistical, descriptive, and graphical techniques. The normality of the continuous variables was assessed with the Shapiro-Wilk's test. Categorical variables were computed using percentages and frequencies, whilst continuous variables were presented using means and standard deviations. The ANOVA and Mann-Whitney U tests were used to determine which radiomics features were strongly linked to the occurrence of ECI.

The feature selection process employed LASSO method, which penalised variables of lesser importance and effectively dealt with problems related to multicollinearity and overfitting. The logistic regression models incorporated parameters that had statistical significance in distinguishing between ECI-positive and ECI-negative nodes.

The models' predictive ability was determined by ROC curve analysis, where the AUC values were computed. The calibration and goodness-of-fit of the model were estimated using the Hosmer-Lemeshow test and the Nagelkerke R-square statistic. Statistical significance was approved as a p-value less than 0.05, and was calculated on both sides of the distribution.

RESULTS

A total of 56 female patients diagnosed with breast cancer and metastatic axillary lymph node involvement were included in the study. The mean age was 59 ± 13 years. The distribution of tumour types among the patients was as follows: 46 (82.1%) had invasive ductal carcinoma, 5 (8.9%) had invasive lobular carcinoma, 2 (3.6%) had mixed carcinoma, and 1 (1.8%) each had mucinous carcinoma, metaplastic carcinoma, and secretory breast carcinoma. ECI was observed in 42 (75%) of the lymph nodes.

Measurements were taken from the axillary lymph nodes of all patients, along with a surrounding 3mm perinodal area. A total of 89 radiomics features were extracted and analysed, including 15 morphology, 26 histograms, 18 GLCM, 11 GLRLM, 5 NGTDM, and 14 GLSZM features. Of these, 39 radiomics features showed a statistically significant association with the presence of ECI ($p < 0.05$). These features included four morphological, 12 first-order, four GLCM, nine GLRLM, two NGTDM, and eight GLSZM features (Table I).

After feature selection using LASSO, the most predictive features for ECI were identified as follows: Three morphological features (sphere diameter, surface area, surface-to-volume ratio), four first-order histogram features (mean, maximum grey level, area under the curve, and root mean square), three GLCM features (joint average, sum average, and autocorrelation), four GLRLM features (low-high grey level run emphasis, grey level non-uniformity, short-run low grey level emphasis), one NGTDM feature (coarseness), and one GLSZM feature (zone size entropy).

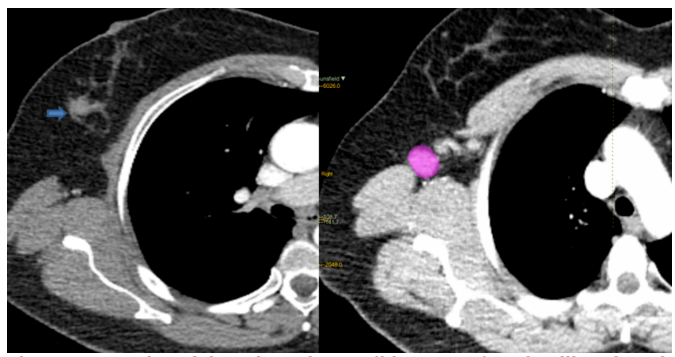

Figure 1: Density of ductal carcinoma (blue arrow) and axillary lymph node segmentation.

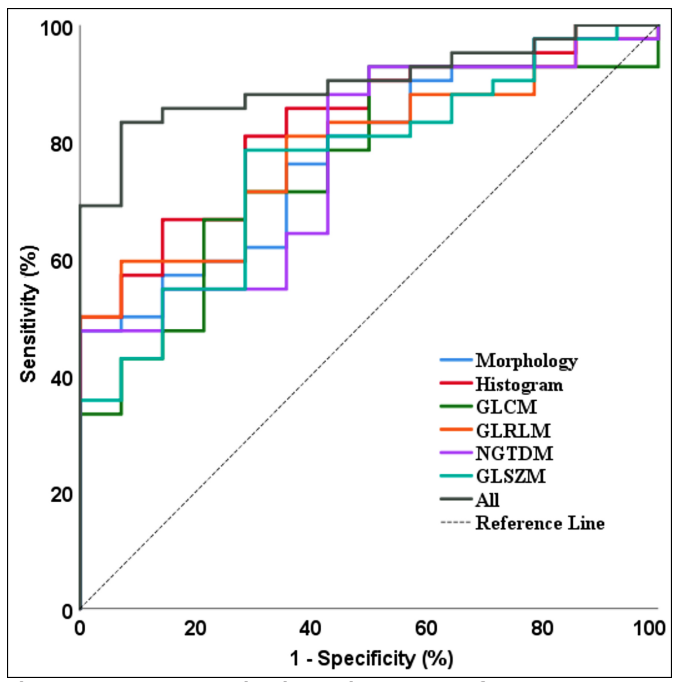

Figure 2: ROC curves used to detect the presence of ECI.

Table I: Radiomics standardised data used in the study.

Characteristics	ECI. No	ECI. Yes	p-value	Characteristics	ECI. No	ECI. Yes	p-value
	Mean ± SD	Mean ± SD			Mean ± SD	Mean ± SD	
Morphology				**GLCM**			
Volume	-0.35 ± 0.11	0.12 ± 1.13	0.130[a]	Joint maximum	0.02 ± 0.94	-0.01 ± 1.03	0.925[a]
Approximate volume	-0.35 ± 0.11	0.12 ± 1.13	0.129[a]	Joint average*‡	-0.51 ± 1.05	0.17 ± 0.93	**0.025**[a]
Voxels counting	-0.34 ± 0.09	0.11 ± 1.13	0.146[a]	Joint variance	-0.30 ± 0.81	0.10 ± 1.05	0.204[a]
Surface area*‡	-0.49 (-0.67; -0.27)[#]	-0.12 (-0.44; 0.29)[#]	**0.003**[b]	Joint entropy log 2	-0.24 ± 1.02	0.08 ± 0.99	0.294[a]
Surface to volume ratio*‡	0.69 ± 1.04	-0.23 ± 0.88	**0.002**[a]	Joint entropy log 10	-0.24 ± 1.02	0.08 ± 0.99	0.294[a]
Compacity	-0.18 ± 0.98	0.06 ± 1.01	0.430[a]	Difference average	-0.03 ± 0.88	0.01 ± 1.05	0.909[a]
Compactness 1	0.22 ± 1.03	-0.07 ± 0.99	0.355[a]	Difference variance	-0.10 ± 0.71	0.03 ± 1.08	0.683[a]
Compactness 2	0.23 ± 1.06	-0.08 ± 0.98	0.322[a]	Difference entropy	-0.24 ± 1.02	0.08 ± 0.99	0.294[a]
Spherical disproportion	-0.19 ± 0.99	0.06 ± 1.01	0.417[a]	Sum average*‡	-0.51 ± 1.05	0.17 ± 0.93	**0.025**[a]
Sphericity	0.21 ± 1.02	-0.07 ± 1.00	0.366[a]	Angular second moment	0.07 ± 1.02	-0.02 ± 1.00	0.760[a]
Asphericity	-0.19 ± 0.99	0.06 ± 1.01	0.417[a]	Contrast	-0.07 ± 0.77	0.02 ± 1.07	0.779[a]
Centre of mass shift	0.09 ± 0.85	-0.03 ± 1.05	0.704[a]	Dissimilarity	-0.03 ± 0.88	0.01 ± 1.05	0.909[a]
Maximum 3D diameter*	-0.57 ± 0.52	0.19 ± 1.05	**0.013**[a]	Inverse difference	-0.05 ± 0.87	0.02 ± 1.05	0.833[a]
Sphere diameter*‡	-0.59 ± 0.45	0.20 ± 1.06	**0.010**[a]	Inverse difference moment	-0.07 ± 0.85	0.02 ± 1.05	0.779[a]
Integrated intensity	-0.22 ± 0.02	0.07 ± 1.15	0.343[a]	Correlation	-0.33 ± 1.11	0.11 ± 0.95	0.152[a]
Histogram				Autocorrelation*‡	-0.51 ± 1.05	0.17 ± 0.93	**0.026**[a]
Mean*‡	-0.48 ± 1.10	0.16 ± 0.92	**0.036**[a]	Cluster shade*	0.46 ± 0.78	-0.15 ± 1.03	**0.046**[a]
variance	-0.38 ± 0.77	0.13 ± 1.04	0.104[a]	Cluster prominence	-0.41 ± 0.61	0.14 ± 1.07	0.079[a]
Skewness*	0.73 ± 0.89	-0.09 ± 0.95	**0.007**[a]	**GLRLM**			
Kurtosis	0.06 ± 1.33	-0.02 ± 0.88	0.804[a]	Short runs emphasis*	0.53 (0.24; 0.67)[#]	0.15 (-0.56; 0.56)[#]	**0.045**[b]
Median*	-0.45 ± 1.05	0.21 ± 0.94	**0.030**[a]	Long runs emphasis*	-0.51 (-0.62; -0.11)[#]	-0.15 (-0.46; 0.65)[#]	**0.047**[b]
Minimum grey level	0.21 ± 1.02	-0.07 ± 1.00	0.367[a]	Low grey level run emphasis*‡	0.47 ± 1.11	-0.16 ± 0.92	**0.043**[a]
10th Percentile*	-0.54 (-0.65; -0.13)[#]	0.28 (-0.54; 0.69)[#]	**0.021**[b]	High grey level run emphasis*‡	-0.48 ± 1.11	0.16 ± 0.92	**0.036**[a]
25th Percentile*	-0.52 (-0.85; -0.12)[#]	-0.04 (-0.52; 1.09)[#]	**0.038**[b]	Short run low grey level emphasis*‡	0.47 ± 1.05	-0.16 ± 0.94	**0.039**[a]
50th Percentile*	-0.57 (-1.27; 0.47)[#]	0.12 (-0.43; 1.03)[#]	**0.037**[b]	Short run high grey level emphasis*	-0.59 (-1.22; 0.05)[#]	0.22 (-0.50; 0.58)[#]	**0.024**[b]
75th Percentile*	-0.52 ± 1.00	0.17 ± 0.95	**0.023**[a]	Long run low grey level emphasis	-0.07 ± 0.57	0.02 ± 1.11	0.759[a]
90th Percentile*	-0.53 ± 0.91	0.18 ± 0.97	**0.019**[a]	Long run high grey level emphasis*	-0.70 (-0.90; -0.09)[#]	-0.23 (-0.46; 0.68)[#]	**0.039**[b]
Standard deviation	-0.39 ± 0.90	0.13±1.01	0.092[a]	Grey level non-uniformity*‡	-0.34 (-0.36; -0.26)[#]	-0.26 (-0.33; -0.08)[#]	**0.021**[b]
Maximum grey level*‡	-0.62 ± 0.62	0.21±1.02	**0.006**[a]	Run length non-uniformity	-0.33 ± 0.10	0.11 ± 1.13	0.152[a]
Mode	-0.24 ± 0.99	0.08±1.00	0.298[a]	Run percentage*	0.56 (0.27; 0.67)[#]	0.19 (-0.53; 0.55)[#]	**0.047**[b]
Interquartile range	-0.26 ± 1.02	0.09 ± 0.99	0.256[a]	**NGTDM**			
Range*	-0.56 ± 0.65	0.19 ± 1.03	**0.015**[a]	Coarseness*‡	0.57 ± 1.16	-0.19 ± 0.88	**0.013**[a]
Mean absolute deviation	-0.35 ± 0.95	0.12 ± 1.00	0.127[a]	Contrast*	0.41 (0.00; 0.91)[#]	-0.07 (-0.82; 0.39)[#]	**0.018**[b]
Robust mean absolute deviation	-0.30 ± 1.00	0.10 ± 0.99	0.191[a]	Busyness	-0.33 ± 0.15	0.11 ± 1.13	0.151[a]
Median absolute deviation	-0.34 ± 0.96	0.11 ± 1.00	0.145[a]	Complexity	-0.32 ± 0.43	0.11 ± 1.11	0.172[a]
Coefficient of variation	-0.32 ± 0.96	0.11 ± 1.00	0.171[a]	Strength	0.26 ± 0.65	-0.09 ± 1.09	0.262[a]
Quartile coefficient of dispersion	-0.21 ± 1.05	0.07 ± 0.99	0.370[a]	**GLSZM**			
Entropy log 10	-0.41 ± 1.04	0.14 ± 0.96	0.080[a]	Small zone emphasis	-0.12 ± 0.84	0.04 ± 1.06	0.621[a]
Entropy log 2	-0.41 ± 1.04	0.14 ± 0.96	0.080[a]	Large zone emphasis*	-0.30 (-0.30; -0.28)[#]	-0.29 (-0.30; -0.17)[#]	**0.039**[b]
Area under curve*‡	-0.48 ± 1.10	0.16 ± 0.92	**0.036**[a]	Low gray level zone emphasis*	0.57 (0.00; 1.20)[#]	-0.12 (-0.81; 0.40)[#]	**0.025**[b]
Uniformity	0.29 ± 1.17	-0.10 ± 0.93	0.211[a]	High gray level zone emphasis*	-0.57 (-1.12; 0.02)[#]	0.20 (-0.51; 0.67)[#]	**0.024**[b]
Root mean square*‡	0.70 ± 1.05	-0.23 ± 0.88	**0.002**[a]	Small zone low grey level emphasis	0.08 ± 0.97	-0.03 ± 1.02	0.721[a]
				Small zone high grey level emphasis	-0.29 ± 0.85	0.10 ± 1.03	0.207[a]
				Large zone low grey level emphasis*	-0.30 (-0.30; -0.28)[#]	-0.28 (-0.29; -0.15)[#]	**0.031**[b]
				Large zone high grey level emphasis*	-0.31 (-0.31; -0.29)[#]	-0.29 (-0.30; -0.14)[#]	**0.021**[b]
				Grey level non-uniformity	-0.34 ± 0.15	0.11 ± 1.13	0.149[a]
				Zone size non-uniformity	-0.37 ± 0.14	0.12 ± 1.13	0.115[a]
				Zone percentage*	0.50 (0.35; 0.70)[#]	-0.01 (-0.81; 0.54)[#]	**0.018**[b]
				Grey level variance	-0.45 ± 0.60	0.15 ± 1.07	0.050[a]
				Zone size variance*	-0.30 (-0.30; -0.28)[#]	-0.28 (-0.30; -0.15)[#]	**0.015**[b]
				Zone*‡	-0.66 ± 0.87	0.22 ± 0.95	**0.003**[a]

** Parameters with statistically significant differences (p <0.05, <0.01, and p <0.001) depending on the presence of ECI in the comparisons made before the LASSO analysis. These parameters, which make a difference in the presence of ECI, were included in the LASSO analysis‡ Data selected for modelling with LASSO analysis; a, One way ANOVA analysis; b, Mann-Whitney U test; #median (interquantile range).*

Table II: Performances of radiomics models used to detect the presence of ECI.

Variables	AUC (95% CI)	Accuracy	Sensitivity	Specificity	Precision	R^2_N
Morphology	0.78 (0.65-0.90)	0.750	0.929	0.214	0.780	0.288
Histogram	0.82 (0.70-0.95)	0.768	0.929	0.286	0.796	0.282
GLCM	0.77 (0.61-0.92)	0.821	0.952	0.429	0.833	0.256
GLRLM	0.86 (0.76-0.96)	0.768	0.881	0.429	0.822	0.343
NGTDM	0.76 (0.63-0.90)	0.750	0.952	0.143	0.769	0.157
GLSZM	0.76 (0.63-0.89)	0.768	0.952	0.214	0.784	0.225
All	0.92 (0.85-0.99)	0.839	0.881	0.714	0.902	0.578

AUC: Area under the curve. CI: Confidence interval. R^2_N: Nagelkerke R-square.

Logistic regression models developed using the selected radiomics features were evaluated for their diagnostic performance. ROC curve analysis showed that the model with all combined features had the highest AUC value of 0.92 (Figure 2). This model also demonstrated an accuracy of 0.839, a specificity of 0.714, and a sensitivity of 0.881. The Nagelkerke R-square value indicated that the combined model explained 57.8% of the variance in ECI status (Table II).

When evaluating individual models, the GLRLM features model achieved the highest AUC of 0.86, while the GLCM feature model showed the highest sensitivity (0.952), specificity (0.429), accuracy (0.821), and precision (0.833). The GLRLM feature model best fits the dependent variable, with a Nagelkerke R-square value of 0.343. Despite these individual performances, no statistically significant difference in AUC values was observed among the independent models ($p > 0.05$). The combined model outperformed all individual models in terms of both AUC and overall diagnostic performance.

DISCUSSION

The findings of this study highlight the potential of radiomics in predicting ECI in metastatic axillary lymph nodes in breast cancer. By leveraging advanced computational techniques to analyse CT images, the authors identified a set of radiomics features significantly correlated with ECI. The combined model, which integrates multiple radiomics features, demonstrated superior diagnostic performance compared to individual feature models, emphasising the importance of a multifaceted approach in medical imaging analysis.

This study contributes to the growing body of literature supporting radiomics in cancer prognosis and diagnosis. The deep learning radiomics of ultrasonography (DLRU) model has shown strong performance in identifying metastatic risk in sentinel and non-sentinel lymph nodes in breast cancer.[17] Hwang *et al*. conducted a study to determine the predictive value of texture analysis (TA) features related to the heterogeneity of axillary lymph nodes using 18F-FDG PET/CT in patients with locally advanced breast cancer. They discovered that skewness, a measure of asymmetry, independently predicts disease progression.[18]

The specific application of radiomics to predict ECI in breast cancer has also been explored in recent studies. For example, Li *et al*. found that certain texture features extracted from ultrasound images were significantly associated with ECI in breast cancer patients. The preset study extends these findings by utilising CT imaging, which provides a different set of radiomics features and offers a more comprehensive view of the tumour micro-environment.[19]

The ability to predict ECI using radiomics features has significant clinical implications. ECI is a known indicator of aggressive disease and poorer prognosis. Accurate prediction of ECI can aid in treatment planning, allowing for more tailored and effective therapeutic strategies. For example, patients identified as having a high risk of ECI may benefit from more aggressive surgical approaches or adjuvant therapies.[20]

Despite the promising results, this study has some limitations. First, the retrospective design may introduce selection bias. Second, the relatively small sample size may limit the generalisability of the findings. Larger, multi-centre studies are needed to validate the preset study's results and ensure their applicability across diverse clinical settings. Third, the manual delineation of ROIs is subjected to inter-observer variability, which may affect the reproducibility of radiomics features. Future studies should consider automated or semi-automated segmentation techniques to improve consistency. Additionally, while the authors used advanced statistical methods such as LASSO for feature selection, the risk of overfitting remains, particularly with high-dimensional data. Robust validation techniques, including external validation cohorts, are essential to confirm the reliability of the predictive models. As this is a single-centre study with a small sample size, future research should focus on increasing the sample size and incorporating multi-centre cohorts to enhance the robustness and generalisability of the findings.

CONCLUSION

This study demonstrates that radiomic features derived from CT images can effectively predict ECI in breast cancer patients with axillary lymph node involvement.

ETHICAL APPROVAL:

Ethical approval was obtained from the Institutional Ethics Review Board of the Oncology Training and Research Hospital before the commencement of the study (IERB No: 04/58-2024).

The study was conducted in compliance with the Declaration of Helsinki and adhered to all applicable ethical guidelines and regulations.

PATIENTS' CONSENT:

Signed consents were taken from all eligible study participants.

COMPETING INTEREST:

The authors declared no conflict of interest.

AUTHORS' CONTRIBUTION:

EB: Conception, design, acquisition, analysis, and interpretation of the data.

EYB: Drafting of the work and revision of the manuscript critically for important intellectual content.
AB: Final approval of the version.
ST: Agreement to be accountable for all aspects of the work in ensuring that questions related to the accuracy or integrity of any part of the work are appropriately investigated and resolved.
All authors approved the final version of the manuscript to be published.

REFERENCES

1. Lukasiewicz S, Czeczelewski M, Forma A, Baj J, Sitarz R, Stanislawek A. Breast cancer-epidemiology, risk factors, classification, prognostic markers, and current treatment strategies-an updated review. *Cancers (Basel)* 2021; **13 (17)**:4287. doi: 10.3390/cancers13174287.
2. Mehdi I, Monem AA, Al Bahrani B, Ramadhan FA. Breast cancer molecular subtypes in Oman: Correlation with age, histology, and stage distribution - analysis of 542 cases. *Gulf J Oncolog* 2014; **1(15)**:38-48.
3. Burguin A, Diorio C, Durocher F. Breast cancer treatments: Updates and new challenges. *J Pers Med* 2021; **11(8)**:808. doi: 10.3390/jpm11080808.
4. Ribnikar D, Ribeiro JM, Pinto D, Sousa B, Pinto AC, Gomes E, *et al*. Breast cancer under age 40: A different approach. *Curr Treat Options Oncol* 2015; **16(4)**:16. doi: 10.1007/s11864-015-0334-8.
5. Layse de Menezes Dantas M, Hugo da Silva Santos Y, Alcantara da Silva PH, Medeiros de Azevedo F, Petta TB, Sampaio Marinho Navarro DT. Prevalence of extracapsular extension in metastatic sentinel lymph nodes in breast cancer. *Surg Oncol* 2021; **38**:101594. doi: 10.1016/j.suronc.2021.101594.
6. Nowikiewicz T, Kurylcio A, Glowacka-Mrotek I, Szymankiewicz M, Novikiewicz M, Zegarski W. Clinical relevance of a degree of extracapsular extension in a sentinel lymph node in breast cancer patients: A single-centre study. *Sci Rep* 2021; **11(1)**:8982. doi: 10.1038/ s41598-021-88351-z.
7. Maraz R, Venczel L, Sikorszki L, Ambrozay E, Serfoza O, Rajtar M *et al*. The importance of the extracapsular extension of the sentinel node metastasis in the surgical treatment of breast cancer. *Magy Seb* 2020; **73(1)**:16-22. doi: 10.1556/1046.73.2020.1.2.
8. Freitas GB, Mota BS, Maesaka JY, Pinheiro CC, de Lima LGCA, Soares JM Jr, *et al*. Measurement of extracapsular extension in sentinel lymph node as a possible predictor of residual axillary disease in breast cancer. *Clinics (Sao Paulo)* 2023; **78**:100216. doi: 10.1016/j.clinsp.2023.100216.
9. Bi WL, Hosny A, Schabath MB, Giger M, Birkbak NJ, Mehrtash A *et al*. Artificial intelligence in cancer imaging: Clinical challenges and applications. *CA Cancer J Clin* 2019; **69(2)**:127-57. doi: 10.3322/caac.21552.
10. Hosny A, Parmar C, Quackenbush J, Schwartz LH, Aerts HJWL. Artificial intelligence in radiology. *Nat Rev Cancer* 2018; **18(8)**:500-10. doi: 10.1038/s41568-018-0016-5.
11. Russo L, Charles-Davies D, Bottazzi S, Sala E, Boldrini L. Radiomics for clinical decision support in radiation oncology. *Clin Oncol (R Coll Radiol)* 2024; **36(8)**:e269-81. doi: 10.1016/j.clon.2024.03.003.
12. Nie K, Al-Hallaq H, Li XA, Benedict HS, Sohn JW, Moran JM, *et al*. NCTN assessment on current applications of radiomics in oncology. *Int J Radiat Oncol Biol Phys* 2019; **104(2)**:302-15. doi: 10.1016/j.ijrobp.2019.01.087.
13. Schick U, Lucia F, Bourbonne V, Dissaux G, Pradier O, Jaouen V, *et al*. Use of radiomics in the radiation oncology setting: Where do we stand and what do we need?. *Cancer Radiother* 2020; **24(6-7)**:755-61. doi: 10.1016/j.canrad.2020.07.005.
14. Aerts, HJ, Velazquez, ER, Leijenaar, RT, Chintan P, Patrick G, Sara C, *et al*. Decoding tumour phenotype by non-invasive imaging using a quantitative radiomics approach. *Nat Commun* 2014; **5(1)**:4006. doi: 10.1038/ncomms5006.
15. Lambin, P, Valezquez ER, Leijenaar R, Carvalho S, Van Striphout RG, Granton P, *et al*. Radiomics: Extracting more information from medical images using advanced feature analysis. *Eur J Cancer* 2012; **48(4)**:441-6. doi: 10.1016/j.ejca.2011.11.036.
16. Fournier L, Costaridou L, Bidaut L, Michoux N, Lecouvet FE, de Geus-Oei LF, *et al*. Incorporating radiomics into clinical trials: Expert consensus endorsed by the European society of radiology on considerations for data-driven compared to biologically driven quantitative biomarkers. *Eur Radiol* 2021; **31(8)**:6001-12. doi: 10.1007/s00330-020-07598-8.
17. Guo X, Liu Z, Sun C, Zhang L, Wang Y, Li Z, *et al*. Deep learning radiomics of ultrasonography: Identifying the risk of axillary non-sentinel lymph node involvement in primary breast cancer. *EBioMedicine* 2020; **60**:103018. doi: 10.1016/j.ebiom.2020.103018.
18. Hwang JP, Choi JY, Choi JH, Cho YS, Hur SM, Kim Z, *et al*. Prognostic value of axillary lymph node texture parameters measured by pretreatment 18f-fluorodeoxyglucose positron emission tomography/computed tomography in locally advanced breast cancer with neoadjuvant chemotherapy. *Diagnostics (Basel)* 2022; **12(10)**:16012. doi: 10.3390/diagnostics12102285.
19. Li H, Zhu Y, Burnside ES, Huang E, Drukker K, Hoadley KA, *et al*. Quantitative MRI radiomics in the prediction of molecular classifications of breast cancer subtypes in the TCGA/TCIA data set. *NPJ Breast Cancer* 2019; **2(1)**:16012. doi: 10.1038/npjbcancer.2016.12.
20. Shigematsu H, Taguchi K, Koui H, Onho S. Clinical significance of extracapsular ınvasion at sentinel lymph nodes in breas cancer patients with sentinel lymph node ınvolvement. *Ann Surg Oncol* 2015; **22(7)**:2365-71. doi: 10.1245/s10434-014-4269-2.